Carbohydrate Polymers 89 (2012) 551–557

Contents lists available at SciVerse ScienceDirect

Carbohydrate Polymers

journal homepage: www.elsevier.com/locate/carbpol

Highly flexible magnetic composite aerogels prepared by using cellulose nanofibril networks as templates

Shilin Liu*, Qiufang Yan, Dandan Tao, Tengfei Yu, Xiaoya Liu

The Key Laboratory of Food Colloids and Biotechnology, Ministry of Education, and School of Chemical and Material Engineering, Jiangnan University, Wuxi 214122, China

ARTICLE INFO

Article history:
Received 15 February 2012
Received in revised form 11 March 2012
Accepted 14 March 2012
Available online 23 March 2012

Keywords:
Cellulose
Aerogels
Magnetic
$CoFe_2O_4$

ABSTRACT

Nanostructured cellulose nanofibrils can form ductile or tough networks that are suitable templates for the creation of materials with functional properties. In this work, a facile method has been developed for the preparation of magnetic hybrid cellulose aerogels. The preparation processes followed by two steps, firstly, preparation of cellulose hydrogel films from LiOH/urea solvent, then $CoFe_2O_4$ nanoparticles were synthesized in the porous structured cellulose scaffolds. After being freeze-dried, $CoFe_2O_4$/cellulose magnetic aerogels were obtained. The porosity of the composite aerogels ranged from 78 to 52% with pore size distribution in a few tens of nanometers. The internal specific surface areas were around 300–320 m^2/g, and the densities were in the range of 0.25–0.39 g/cm^3. The hybrid aerogels showed improved mechanical strength, superparamagnetic properties. Unlike solvent-swollen gels and ferrogels, the magnetic composite aerogels were lightweight, flexibility, high porosity and with large specific surface area and could be expected to be used in many fields.

1. Introduction

Aerogels are materials prepared by replacing the liquid solvent in a gel with air without substantially altering the network structure or the volume of the gel body. This type of materials can be synthesized with porosity up to 99.9%, making them have extraordinarily high in surface area and ultralow in density. Owing to their unique topological porous structure, aerogels have many exciting properties, including ultralow density, high specific surface area, unique optical and acoustic properties, low dielectric permittivity, as well as extraordinarily low thermal conductivity (Carta et al., 2009; Ge, Yang, Li, & Zhao, 2009; Hüsing & Schubert, 1998; Kistler, 1931; Oh, Kim, & Kim, 2009), holding 15 entries in *Guinness World Records* for material properties.

Cellulose aerogels, as the "young" third generation succeeding the inorganic and synthetic polymer-based aerogels, are intriguing materials because of being one of the most abundant and renewable natural polymers. Moreover, it promises a very low density as typical for aerogels but also a comparatively high strength and ductility compared with inorganic or polymeric aerogels (Liebner, Potthast, Rosenau, Haimer, & Wendland, 2008; Olsson et al., 2010; Pääkkö et al., 2008). In general, shaped cellulose aerogels can be prepared from native cellulose nanofibers that isolated from a range of renewable bio-sources (Aulin, Netrval, Wågberg, & Lindström, 2010; Gawryla, Van den Berg, Weder, & Schiraldi, 2009; Korhonen, Hiekkataipale, et al., 2011; Korhonen, Kettunen, Ras, & Ikkala, 2011; Sehaqui, Salajková, Zhou, & Berglund, 2010), or regenerated cellulose that by dissolving native cellulose in direct solvents (Gavillon & Bustova, 2008; Hoepfner, Ratke, & Milow, 2008; Liebner et al., 2009; Sescousse, Smacchia, & Budtova, 2010; Sescousse, Gavillon, & Budtova, 2011), or from microbial (bacterial) cellulose that produced by some bacteria (Chen, Ushida, & Tateishi, 2002; Liebner et al., 2010; Whang, Thomas, Healy, & Nuber, 1995). Different cellulose sources and preparation methods make the aerogel materials with totally different microstructures and properties. Nowadays, the pursuit for functional cellulose aerogels has become a hot research topic which has stimulated a variety of studies describing different approaches for material engineering. Several studies have also been carried out on the preparation of cellulose aerogels with superhydrophobic (Jin et al., 2011), electrical (Ikkala et al., 2009), improved mechanical (Svagan, Berglund, & Jensen, 2011), or magnetic properties (Pääkkö et al., 2008). It is believed that the new combinations of properties can be extended to new applications by the introduction of new chemical compositions with deliberately prepared micro- and nano-structures.

In our previous work, novel aqueous solvents contained alkali and urea have been developed for cellulose dissolving. Moreover, regenerated cellulose materials including films (Liu, Zhang, Sun, Lin, & Nishiyama, 2009; Liu, Zeng, Tao, & Zhang, 2010), fibers (Li et al., 2010) and microspheres (Luo, Liu, Zhou, & Zhang, 2009) with novel structure and properties have been prepared successfully from the cellulose dope. It was worth noting that the cellulose films

* Corresponding author. Tel.: +86 510 85917090; fax: +86 510 85917763.
E-mail address: slliu2009@jiangnan.edu.cn (S. Liu).

0144-8617/$ – see front matter © 2012 Elsevier Ltd. All rights reserved.
doi:10.1016/j.carbpol.2012.03.046

at wet state exhibited homogeneous porous structure, which could be used as nano-reacting sites where inorganic nanoparticles could be synthesized in situ (Liu, Ke et al., 2011; Liu, Zhou, Zhang, Guan, & Wang, 2006; Liu, Zhang, Zhou, & Wu, 2008; Liu, Zhou, Zhang, Xiang, et al., 2008; Liu, Zhou, & Zhang, 2011a, 2011b;). In the current work, we proposed a facile approach for the non-agglomerated growth of cobalt ferrite nanoparticles by using regenerated cellulose nanofibril networks as templates. This method allowed the synthesized nanoparticles with different contents and small particle size in cellulose scaffolds. It was a quite different method compared with the reported works, and the obtained materials were based on native resources, meeting the basic requirements of green chemistry. Moreover, unlike solvent-swollen gels and ferrogels, the magnetic composite aerogel was lightweight, porous, and flexible, and had improved compression strength, superparamagnetic properties and low thermal conductivity. Owing to the flexibility, high porosity and surface area, these aerogels are expected to be useful in microfluidics devices and as electronic actuators. We hope the interesting properties will help, not only for the fabrication of new magnetic composites and the development of spatially confined synthetic approaches, but also for the acquiring additional understanding of the physicochemical processes occurring in a confined environment.

2. Experimental

2.1. Chemicals

Cotton linter pulp (α-cellulose > 95%) was provided by Hubei Chemical Fiber Group Ltd. (Xiangfan, China), its viscosity-average molecular weight (M_η) was determined to be 1.03×10^5 according to the reported method. Other chemical reagents with analytical grade were supplied by the Sinopharm Chemical Reagent Co. Ltd. (China) and used without further purification.

2.2. Preparation of regenerated cellulose hydrogel membrane

The freezing–thawing method was used for cellulose dissolving. Briefly, cotton linter pulp (native cellulose) was dispersed into aqueous lithium hydroxide/urea solution (4.6 wt%/15.0 wt%), and then put it in a refrigerator, after it had been frozen, took it out and thawed at room temperature to obtain transparent cellulose solution (5 wt%). The resultant cellulose solution was subjected to centrifuge at 7500 rpm and 15 °C for 10 min to eliminate some bubbles in the viscous solution. The bubble-free solution was cast on a glass plate and the thickness of the solution was controlled to be about 0.25 mm, and then immersed into coagulation bath containing 80 vol% ethanol to coagulate and regenerated for 10 min. The regenerated cellulose (RC) membranes were washed with deionized water, and kept them at swollen state before using.

2.3. Preparation of magnetic cellulose aerogels

The obtained cellulose hydrogel membranes were immersed in freshly prepared aqueous solutions of $FeCl_3$ and $CoCl_2$ with a molar ratio of [Fe]/[Co] = 2 for 24 h, it was allowed a homogeneous distribution of the precursor solution obtained inside the cellulose networks. The hydrogel membranes contained precursor solution was subsequently treated with NaOH solution (2 mol/L). The color of the samples changed from red/orange to black immediately, and inorganic nanoparticles formed in the cellulose matrix. The composite cellulose membranes were washed with water to remove counter-ions, and then freeze-dried. The composite aerogels prepared from $CoCl_2$ salts with concentrations of 0.01, 0.03, 0.06 and 0.1 mol/L were coded as RCF-001, RCF-003, RCF-006, and RCF-01, respectively ([Fe]/[Co] = 2). The aerogels prepared from regenerated cellulose membranes by using the same method were coded as RC.

2.4. Characterization

Wide-angle X-ray diffraction (XRD) measurement was carried out on a XRD diffractometer (D8-Advance, Bruker, USA). The patterns with Cu Kα radiation at 40 Kv and 30 mA were recorded in the region of 2θ from 5° to 70°. Samples were cut into powders and dried in vacuum oven at 60 °C for 48 h. Thermal gravimetric analysis (TGA) was performed with a thermogravimetric analysis (Netzsch, Germany). About 5 mg of the tested samples were placed in a platinum pan and heated from 20 to 700 °C at a rate of 10 K min^{-1} in air atmosphere. Nitrogen adsorption measurements were performed with a Quantachrome NOVA 4200e (USA), Brunauer–Emmett–Teller (BET) and Barrett–Joyner–Halendar (BJH) analysis were performed with the autosorb program (Quantachrome). BET analysis was carried out for a relative vapor pressure of 0.05–0.3 at 77 K. BJH analysis was performed from the desorption branch of the isotherms. Scanning electron microscopy (SEM) tests were carried out by using a Hitachi S-4800 microscope. For transmission electron microscopy (TEM), the gel specimens were embedded in a poly(methylmethacrylate-butylmethacrylate) (PMMABMA) resin. In this procedure, the water in the aerogels was exchanged with ethanol, which was then exchanged with the mixed monomers. The aerogels was immersed in the mixed monomer directly. The embedded specimen was sectioned with a Leica Ultracut-E using a glass knife. The sections of approximately 100 nm thickness were mounted on a grid with carbon support, and then disembodied by removing the resin with acetone. The section was then examined with a TEM (JEOL-1010) apparatus. The bulk density of the aerogels was obtained by measuring the volume and weight of carved aerogels. The porosity was calculated by using the formula: $Pr = (1 - \rho_m/\rho_t) \times 100\%$ (Wei, Lu, & Chang, 2009), and ρ_m was the apparent density of the final product and ρ_t was the combined density of the $CoFe_2O_4$ and cellulose at a specified ratio. The mechanical properties of the aerogels were characterized on a Shimadzu Autograph AG-I 100 kN by using compressing tests. For compression test, cellulose and composite aerogels with thickness about 1 cm were prepared through the same way. The magnetic properties of the composite aerogels were evaluated with a superconducting quantum interference device (SQUID, MPMS XL-7, QUANTUM DESIGN, USA) at 298 K, and the hysteretic loop was obtained in a magnetic field that varied from −7 to +7 T.

3. Results and discussion

The composite aerogels were prepared by in situ synthesis of $CoFe_2O_4$ nanoparticles in the cellulose matrix. The morphology and structure of the RC hydrogel film had homogeneous macroporous structure, which was shown in Fig. 1. This unique structure could be ascribed to the phase separation of the cellulose solution during the regenerating process, where solvent-rich regions contributed to the pores formation. The pore size distribution was in the mesopore and macropore ranges, and the S_{BET} of the cellulose aerogels was about 270 m^2/g. When the porous structured cellulose hydrogel films were immersed into $CoFe_2O_4$ precursor solution, the inorganic ions could be readily impregnated into the cellulose matrix through the pores and interacted with cellulose matrix. After being treated with NaOH, the color of the cellulose membranes turned brown or black, indicating that inorganic nanoparticles had been synthesized in the cellulose matrix.

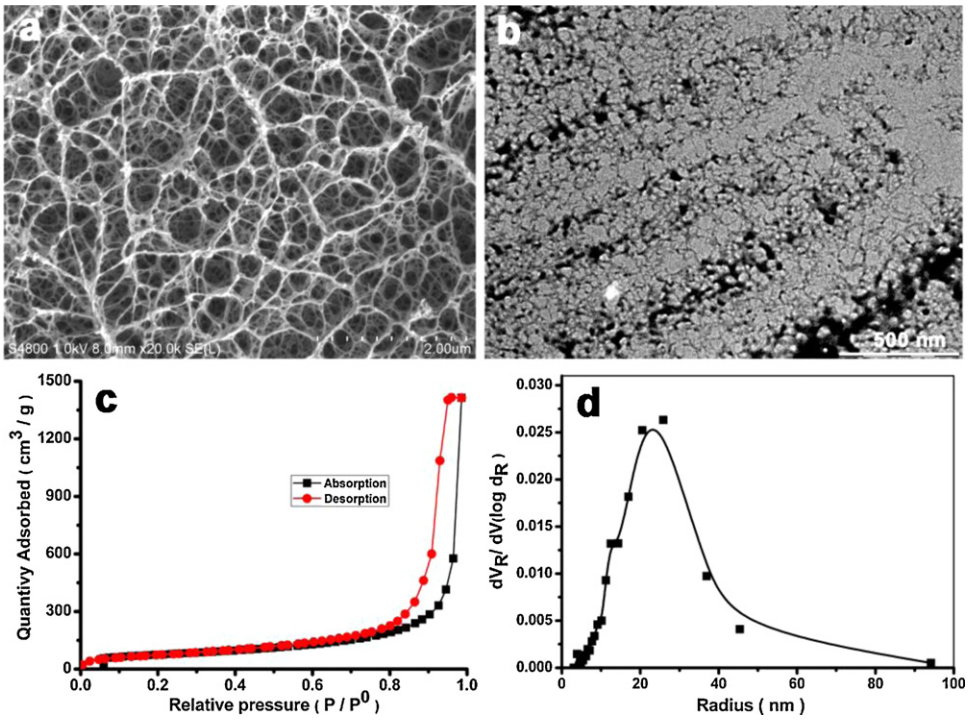

Fig. 1. SEM (a) and TEM (b) images of cellulose xerogel after freeze-dried with liquid nitrogen, and nitrogen adsorption–desorption isotherm of the cellulose xerogel (c), with the BJH pore size distribution of the cellulose xerogel (d).

Fig. 2 shows the surface morphologies of the composite aerogels. Inorganic nanoparticles were located on the cellulose nanofibril surfaces. All of the samples showed bicontinuous distribution of interconnected particles and macropores. It was obvious that a small quantity of inorganic nanoparticles (Fig. 2a) had an obvious influence on the microstructure of the aerogels, indicating that cellulose nanofibrils acted as reacting sites, conditioning the growth of the inorganic nanoparticles. As a result, a more branched, granular-like structure was obtained. While for the pristine cellulose aerogels, the cellulose nanofibrils connected to each other and formed three-dimensional scaffold, and the formed pores were more open. These pores could anchor the nanoparticles and provide channels for the facile migration of the reactants and by-products from the chemical reactions.

In order to further clarify the structure of the composite aerogels, TEM images of the aerogels was carried out by ultrathin

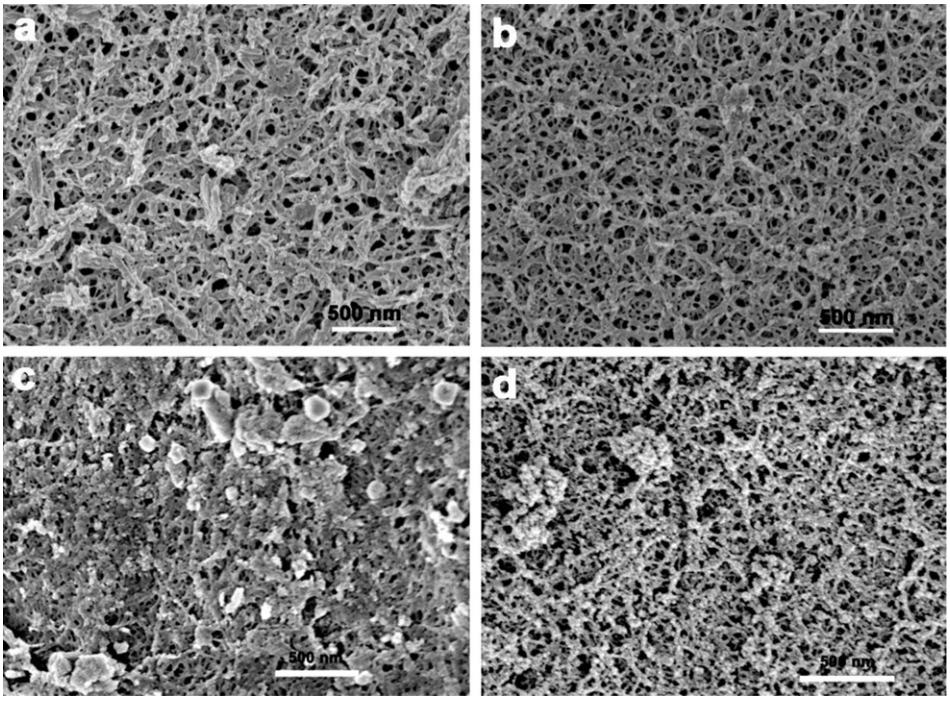

Fig. 2. SEM images of the composite aerogels; (a–d) were for RCF-001, RCF-003, RCF-006, and RCF-01, respectively.

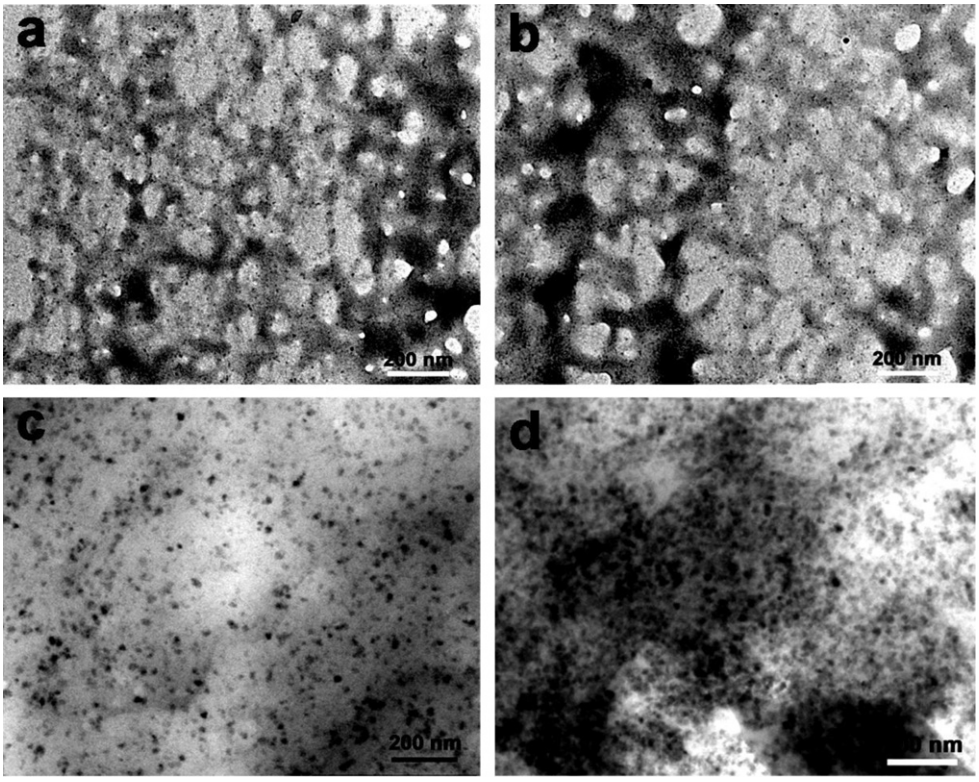

Fig. 3. TEM images of the composite aerogels; (a–d) were for RCF-001, RCF-003, RCF-006, and RCF-01, respectively.

sectioning of resin-embedded composite aerogels, and then followed by removing of the resin on the TEM grid. Fig. 3 shows the micrographs of the composite aerogels. It could be seen that a large number of $CoFe_2O_4$ nanoparticles with small particle size were uniformly dispersed in the cellulose matrix. As discussed above, the incorporated Co^{2+} and Fe^{3+} ions were bound to cellulose molecules via electrostatic (i.e., ion–dipole) interactions between the electron-rich oxygen atoms in the cellulose molecules and the electropositive transition metal cations. Due to the interactions, the Co^{2+} and Fe^{3+} ions were anchored tightly to the cellulose nanofibrils and depressed the mobility of the Co^{2+} and Fe^{3+} ions on cellulose nanofibrils' surface, enhancing the formation of $CoFe_2O_4$ nuclei and preventing the particles from overgrowth. Collectively, these ionic interactions stabilized the $CoFe_2O_4$ nanoparticles, leading to the uniform distribution of $CoFe_2O_4$ nanoparticles on the cellulose fibril surfaces.

Based on our previous works, it indicated that metal oleation/oxolation was significantly affected in the presence of the cellulose matrix. Condensation reactions proceeded within the interstitial network of cellulose nanofibrils as well as within the adsorbed metal hydroxo/oxo cation layer on the cellulose nanofibrils (formation of precursor). The chemically adsorbed metal hydroxide/oxide ion layer would connect the cellulose nanofibrils surfaces with the metal hydroxo/oxo network complexes in the liquid phase, which possibly allowed for direction of the condensation reactions toward the cellulose nanofibrils surfaces as the condensates formed into ferrite particles (formation of a cellulose–precursor composite). Therefore, non-grafted particles inside the aerogel networks were formed. The inorganic nanoparticles synthesized in the cellulose scaffolds had small particle size and narrow size distribution.

Fig. 4 shows the XRD of the cellulose aerogels and composite aerogels. The peaks at $2\theta = 12.1^\circ$, 20.3°, and 21.8° were ascribed to the $(1\,\bar{1}\,0)$, $(1\,1\,0)$, and $(2\,0\,0)$ planes of cellulose II crystalline, respectively (Isogai, Usuda, Kato, Uryu, & Atalla, 1989). In addition to the peaks of cellulose II, there were some diffraction peaks that related to those of $CoFe_2O_4$ (powder diffraction file, JCPDS card no. 79-1744). The diffraction peaks showed a considerable line broadening due to the low crystallinity or small crystalline size. It further supported that the synthesized nanoparticles with small particle size and agreed well with the results obtained from TEM observation.

The N_2 adsorption–desorption isotherms for determining the characteristic of the aerogels were shown in Fig. 5a–e. The

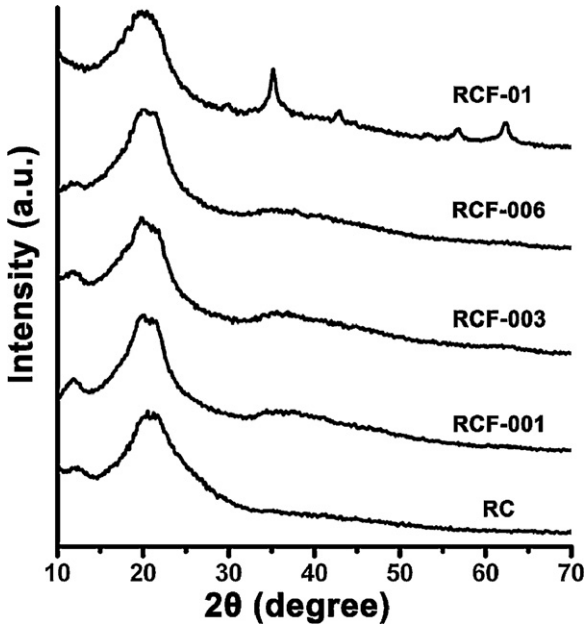

Fig. 4. XRD of cellulose and magnetic composite aerogels.

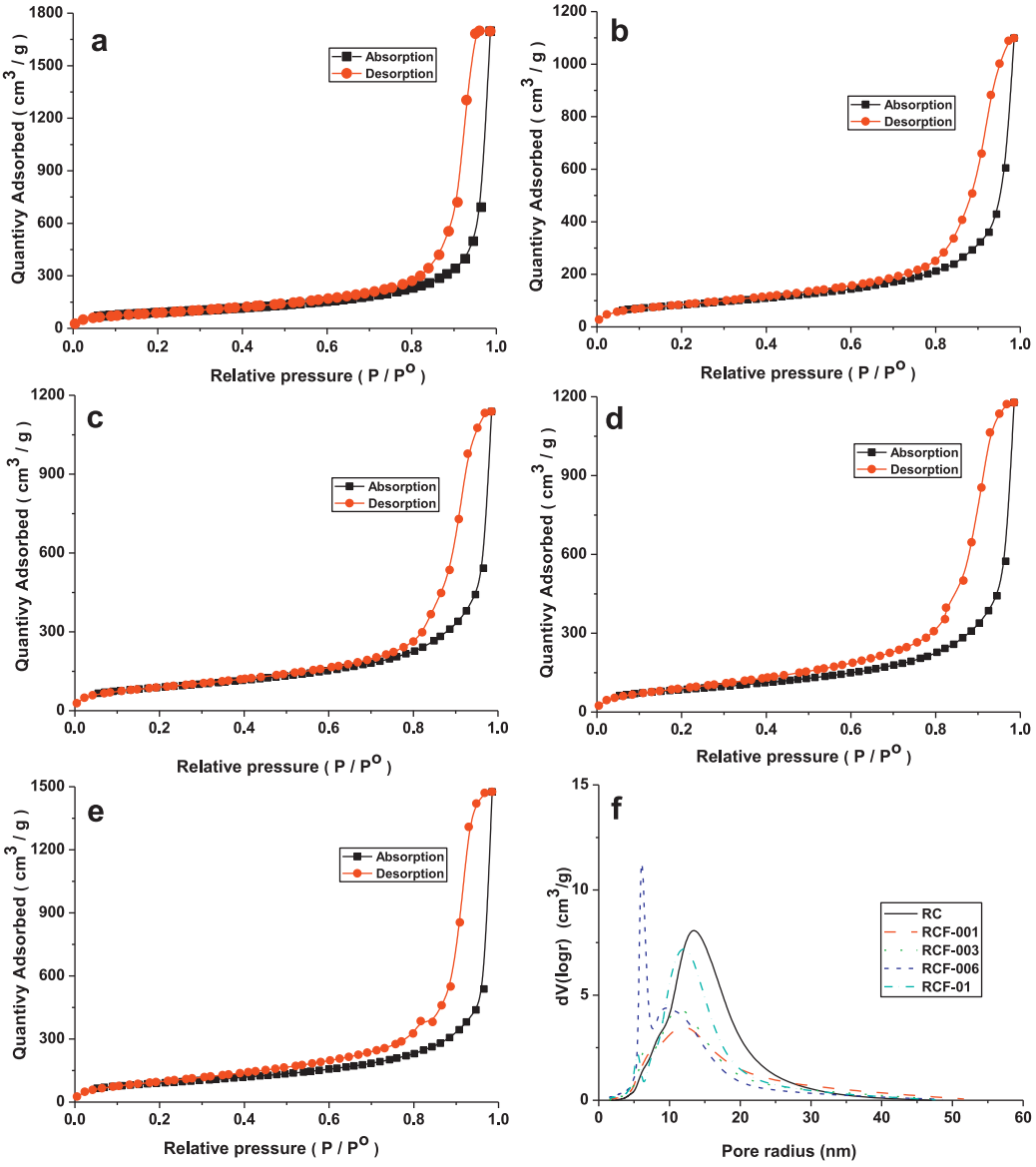

Fig. 5. Nitrogen adsorption–desorption isotherms (a–e) and BJH pore size distribution (from desorption branch) of the cellulose and composite aerogels (f); (a–e) were for RC, RCF-001, RCF-003, RCF-006, and RCF-01, respectively.

isotherms for all samples were classified to type IV according to IUPAC classification, and the broad adsorption–desorption loops were classified to the type H3 (Kruk & Jaroniec, 2001) the sharp nitrogen uptake near P_0 indicated a continuity of the pore size distribution between mesopores and macropores. S_{BET} was inferred from the N_2 adsorption isotherms by a Brunauer–Emmett–Teller analysis of the amount of gas adsorbed at P/P_0 between 0.05 and 0.3, and the data were listed in Table 1. The surface areas were around 300–320 m^2/g and changed slightly with the increasing of the content of $CoFe_2O_4$ nanoparticles, while the porosities of the composite

Table 1
Properties of the cellulose and magnetic composite aerogels.

Sample	$CoFe_2O_4$ content (wt%)[a]	Density (g/cm^3)	Porosity (%)	S_{BET} (m^2/g)[b]	Pore size (nm)[c]	Pore volume (cm^3/g)[c]	Young's modulus (MPa)[d]	λ (mW/m·k)[e]
RC	–	0.218 ± 0.38	82.21 ± 3.27	270.42	31.72	2.71	85.23 ± 9.38	38.44 ± 1.16
RCF-001	2.30	0.254 ± 0.23	78.34 ± 4.06	298.15	14.38	1.72	133.34 ± 11.44	34.91 ± 1.34
RCF-003	3.89	0.262 ± 0.46	72.78 ± 4.74	317.37	20.32	1.78	166.67 ± 10.76	46.63 ± 2.08
RCF-006	5.35	0.311 ± 0.39	63.49 ± 3.98	305.45	12.16	1.88	171.48 ± 8.27	48.55 ± 2.56
RCF-01	10.36	0.390 ± 0.41	52.13 ± 4.31	323.93	20.56	2.37	180.76 ± 11.71	43.17 ± 2.44

[a] Data from TG analysis.
[b] Data obtained from BET with a relative vapor pressure of 0.05–0.3 of desorption branch.
[c] Data from BJH desorption branch.
[d] Data obtained from compression test.
[e] Thermal conductivity values obtained at ambient conditions with thickness about 1 mm.

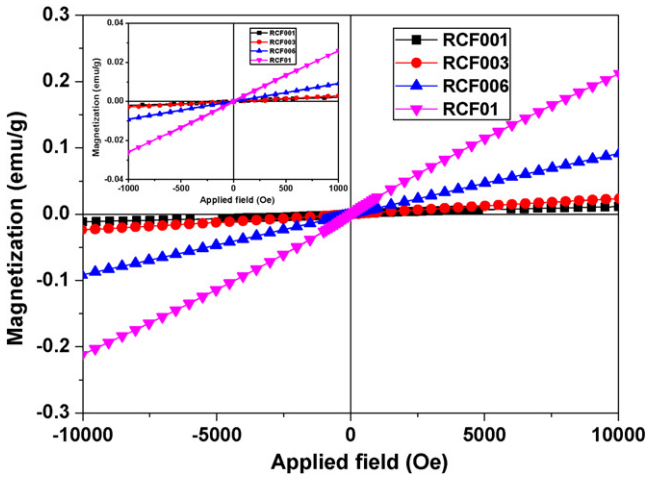

Fig. 6. Hysteresis cycles of the composite aerogels at 298 K; the insert was the initial magnetization curve as a function of applied magnetic field.

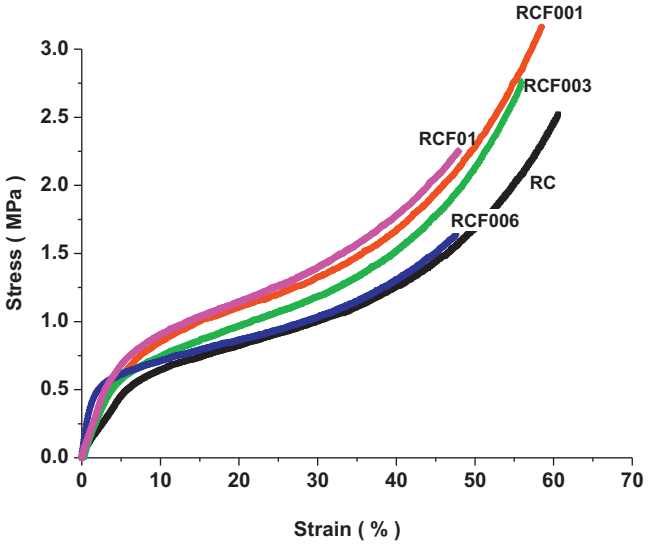

Fig. 7. Compression stress–strain curves of cellulose and composite aerogels.

aerogels decreased from 78 to 52%, and densities increased from 0.25 to 0.39 g/cm^3 with the increasing of the inorganic contents. The decrease in the porosity was ascribed to the incorporated $CoFe_2O_4$ nanoparticles in the porous cellulose matrix, which seemed to result in a decrease in macroporosity. It was found that the pore volume was effectively controlled by the incorporated $CoFe_2O_4$ nanoparticles. The pore volumes decreased from 2.71 cm^3/g for cellulose aerogels to 1.72 cm^3/g for CF-001 drastically, while for the composite aerogels, it increased with the increasing of the content of $CoFe_2O_4$ nanoparticles, but all of them were lower than that of pristine cellulose aerogel. It was also seen from the changed absorbed gas amount in the N_2-absorption isotherms. It was understandable if we considered the role of the cellulose network as a hard template. After incorporated $CoFe_2O_4$ nanoparticles in the cellulose network structure, during the drying process, the composite gels shrank and the pores collapsed, due to the capillary force exerted on the pore wall and the interactions between cellulose matrix and $CoFe_2O_4$ nanoparticles. On the other hand, the composite aerogels with higher content of $CoFe_2O_4$ nanoparticles would be expected to be more resistant to the shrinkage and collapse for the physical volume of the $CoFe_2O_4$ nanoparticles presented in the composite gel. Increasing the content of $CoFe_2O_4$ nanoparticles further resulted in significant decrease in the pore sizes of the composite aerogels. Fig. 5f shows the pore size distribution of the aerogels calculated from the desorption branch. The cellulose aerogels, with mean pore size about 52 nm, showed a broad size distribution, which extended considerably up to 80 nm. While for the composite aerogels, the mean pore size of the composite aerogels decreased, and a little part of smaller pore with pore size about 6 nm were observed. It indicated that $CoFe_2O_4$ nanoparticles had an obvious influence on the microstructure of the cellulose aerogels.

The room-temperature magnetization hysteresis curves of the composite aerogels were measured with superconducting quantum interference device and was shown in Fig. 6. The forward and backward magnetization curves of the aerogels were almost the same. The inset of Fig. 6 showed an expanded view of the curves near the $H = 0$ region, showing that both curves went through the same zero magnetization point at $H = 0$. The absence of hysteresis and coercivity was characteristic of superparamagnetic behavior (Leslie-Pelecky & Rieke, 1996; Sohn & Cohen, 1997). The low crystallinity and small particle size of $CoFe_2O_4$ nanoparticles was considered to be the reason for the low magnetization compared with that of bulk $CoFe_2O_4$. It has been known that magnetic particles, which are smaller than some critical particle size, can be called single domains. As the particle size continues to decrease below the single domain value, the particles exhibit superparamagnetic properties. This result further confirmed that the particle size of the prepared $CoFe_2O_4$ nanoparticles by this method was small. The magnetization of the composite aerogels did not exhibit saturation even in a strong magnetic field of about 20 kOe. The weak magnetization and lack of saturation have often been observed in the magnetic nanoparticles of similar sizes due to the surface and size effects. The discontinuity of the super-exchange between the magnetic cations near or on the nanoparticle surfaces led to the formation of nonlinear spins. The noncollinear spin structure reduced the total magnetic moment of the nanoparticles, leading to the decrease in the magnetization of the nanocomposite aerogels. The remnant magnetizations of the aerogels were near zero, indicating a random distribution of magnetic moments. The monodispersity of $CoFe_2O_4$ nanoparticles in the cellulose aerogels and the persistence of superparamagnetic relaxation of the nanoparticles contributed to the nonsaturation of the magnetization (Nguyen & Diaz, 1994; Tang et al., 1999).

The composite aerogels exhibited striking flexibility, repeated bending through 180° caused no apparent damage, while the inherent drawback of aerogels was typically brittle. The stress–strain curves obtained from compression test for the pure cellulose and composite aerogels was shown in Fig. 7. Composite aerogels could be easily deformed to a large amount before any fracture appears. The stress–strain curves also indicated that the composite aerogels had higher compressibility than that of cellulose aerogels. The instantaneous modulus values calculated at various strain values for each test were shown in Table 1. The modulus value of cellulose aerogel was 85 MPa, it increased from 133 MPa for CF-001 to 180 MPa for CF-01. It indicated that even a low content of $CoFe_2O_4$ contributed to an obvious improvement of the mechanical properties of the material: Young's modulus increased, and the maximum compression strength and the corresponding strain increased. Furthermore, the mechanical behavior improvement was noticeable from the much higher energy that the hybrid aerogels were able to absorb up to the maximum compression strength (roughly the area under the stress–strain curve). Unlike solvent-swollen gels and ferrogels, the magnetic composite aerogels could be expected to be useful in many fields.

4. Conclusions

We have demonstrated a facile method for the preparation of magnetic cellulose aerogels. The magnetic aerogels were light-weight, flexible; the porosities of the composite aerogels were ranged from 78 to 52%. The internal specific surface areas and densities of the aerogels were around 300–320 m^2/g and 0.25–0.39 g/cm^3, respectively. The content of the incorporated $CoFe_2O_4$ nanoparticles increased with the increasing of the $CoFe_2O_4$ precursor concentration, but the particle size changed hardly. The incorporated $CoFe_2O_4$ nanoparticles changed the microstructure of the cellulose aerogels obviously; making it was different from those of the composite aerogels. The hybrid aerogels showed superparamagnetic behaviors, improved mechanical properties with respect to the corresponding inorganic aerogel. Because the concepts of the process were simple and cellulose is sustainable and readily available in large quantities from plants (wood), the suggested route is suitable for industrial-scale production and may be used with many types of nanoparticles, which will open the application fields of cellulose based functional materials.

Acknowledgments

This work was supported by National Natural Science Foundation of China (51003043), and the Fundamental Research Funds for the Central Universities (JUSRP11107) of Jiangnan University.

References

Aulin, C., Netrval, J., Wågberg, L., & Lindström, T. (2010). Aerogels from nanofibrillated cellulose with tunable oleophobicity. *Soft Matter*, *6*, 3298–3305.

Carta, D., Casula, M. F., Corrias, A., Falqui, A., Loche, D., Mountjoy, G., et al. (2009). Structural and magnetic characterization of Co and Ni silicate hydroxides in bulk and in nanostructures within silica aerogels. *Chemical Materials*, *21*, 945–953.

Chen, G. P., Ushida, T., & Tateishi, T. (2002). Scaffold design for tissue engineering. *Macromolecular Bioscience*, *2*, 67–77.

Gavillon, R., & Bustova, T. (2008). Aerocellulose: New highly porous cellulose prepared from cellulose–NaOH aqueous solutions. *Biomacromolecules*, *9*, 269–277.

Gawryla, M. D., Van den Berg, O., Weder, C., & Schiraldi, D. A. (2009). Clay aerogel/cellulose whisker nanocomposites: A nanoscale wattle and daub. *Journal of Materials Chemistry*, *19*, 2118–2124.

Ge, D., Yang, L., Li, Y., & Zhao, J. (2009). Hydrophobic and thermal insulation properties of silica aerogel/epoxy composite. *Journal of Non-Crystalline Solids*, *355*, 2610–2615.

Hoepfner, S., Ratke, L., & Milow, B. (2008). Synthesis and characterisation of nanofibrillar cellulose aerogels. *Cellulose*, *15*, 121–129.

Hüsing, N., & Schubert, U. (1998). Aerogels-airy materials: Chemistry, structure and properties. *Angewandte Chemie International Edition*, *37*, 22–45.

Ikkala, O., Ras, R. H. A., Houbenov, N., Ruokolainen, J., Pääkkö, M., Laine, J., et al. (2009). Solid state nanofibers based on self-assemblies: From cleaving from self-assemblies to multilebel hierarchical constructs. *Faraday Discussions*, *143*, 95–107.

Isogai, A., Usuda, M., Kato, T., Uryu, T., & Atalla, R. H. (1989). Solid-state CP/MAS carbon-13 NMR study of cellulose polymorphs. *Macromolecules*, *22*, 3168–3172.

Jin, H., Kettunen, M., Laiho, A., Pynnönen, H., Paltakari, J., Marmur, A., et al. (2011). Superhydrophobic and superoleophobic nanocellulose aerogel membranes as bioinspired cargo carriers on water and oil. *Langmuir*, *27*, 1930–1934.

Kistler, S. S. (1931). Coherent expanded aerogels and jellies. *Nature (London)*, *127*, 741.

Korhonen, J. T., Hiekkataipale, P., Malm, J., Karppinen, M., Ikkala, O., & Ras, R. H. A. (2011). Inorganic hollow nanotube aerogels by atomic layer deposition onto native nanocellulose templates. *ACS Nano*, *5*, 1967–1974.

Korhonen, J. T., Kettunen, M., Ras, R. H. A., & Ikkala, O. (2011). Hydro-phobic nanocellulose aerogels as floating, sustainable, reusable and recyclable oil absorbents. *ACS Applied Material and Interfaces*, *3*, 1813–1816.

Kruk, M., & Jaroniec, M. (2001). Gas adsorption characterization of ordered orgnic–inorgnic nanocomposite materials. *Chemistry of Materials*, *13*, 3169–3183.

Leslie-Pelecky, D. L., & Rieke, R. D. (1996). Magnetic properties of nanostructured materials. *Chemistry of Materials*, *8*, 1770–1783.

Li, R., Chang, C., Zhou, J., Zhang, L., Gu, W., Li, C., et al. (2010). Primarily industrialized trial of novel fibers spun from cellulose dope in NaOH/urea aqueous solution. *Industrial and Engineering Chemistry Research*, *49*, 11380–11384.

Liebner, F., Haimer, E., Potthast, A., Loidl, D., Tschegg, S., Neouze, M.-A., et al. (2009). Cellulosic aerogels as ultra-lightweight materials. *Holzforschung*, *63*, 3–11.

Liebner, F., Haimer, E., Wendland, M., Neouze, M.-A., Schlufter, K., Miethe, P., et al. (2010). Aeogels from unaltered bacterial cellulose: Application of $scCO_2$ drying for the preparation of shaped ultra-lightweight cellulosic aerogels. *Macromolecular Bioscience*, *10*, 349–352.

Liebner, F., Potthast, A., Rosenau, T., Haimer, E., & Wendland, M. (2008). Cellulose aerogel: Highly porous ultra-lightweight materials. *Holzforschung*, *62*, 129–135.

Liu, S., Ke, D., Zeng, J., Zhou, J., Peng, T., & Zhang, L. (2011). Creation of inorganic nanoparticles by micro-nano-porous structure of cellulose matrix. *Cellulose*, *18*, 945–956.

Liu, S., Zeng, J., Tao, D., & Zhang, L. (2010). Microfiltration performance of regenerated cellulose membrane prepared at low temperature for wastewater treatment. *Cellulose*, *17*, 1159–1169.

Liu, S., Zhang, L., Sun, Y., Lin, Y., & Nishiyama, Y. (2009). Supramolecular structure and properties of high strength regenerated cellulose films. *Macromolecular Bioscience*, *9*, 29–35.

Liu, S., Zhang, L., Zhou, J., & Wu, R. (2008). Structure and properties of cellulose/Fe_2O_3 nanocomposite fibers spum via an effective pathway. *Journal of Physical Chemistry C*, *112*, 4538–4544.

Liu, S., Zhang, L., Zhou, J., Xiang, J., Sun, J., & Guan, J. (2008). Fiber like Fe_2O_3 macroporous nanomaterials fabricated by calcinating regenerated cellulose composite fibers. *Chemistry of Materials*, *20*, 3623–3628.

Liu, S., Zhou, J., & Zhang, L. (2011a). In situ synthesis of plate-like Fe_2O_3 nanoparticles in porous cellulose films with obvious magnetic anisotropy. *Cellulose*, *18*, 663–673.

Liu, S., Zhou, J., & Zhang, L. (2011b). Effects of crystalline phase and particle size on the properties of plate-like Fex nanoparticles during γ- to α-phase transformation. *Journal of Physical Chemistry C*, *115*, 3602–3611.

Liu, S., Zhou, J., Zhang, L., Guan, J., & Wang, J. (2006). Synthesis and alignment of iron oxide nanoparticles in a regenerated cellulose film. *Macromolecular Rapid Communications*, *27*, 2084–2089.

Luo, X., Liu, S., Zhou, J., & Zhang, L. (2009). In situ synthesis of Fe_3O_4/cellulose microspheres with magnetic-induced protein delivery. *Journal of Materials Chemistry*, *19*, 3538–3545.

Nguyen, T., & Diaz, A. (1994). A novel method for the preparation of magnetic nanoparticles in a polyrrole powder. *Journal of Advanced Materials*, *6*, 858–860.

Oh, K. W., Kim, D. K., & Kim, S. H. (2009). Ultra-porous flexible PET/Aerogel blanket for sound absorption and thermal insulation. *Fiber and Polymers*, *10*, 731–737.

Olsson, R. T., Azizi Samir, M. A. S., Salazar-Alvarez, G., Belova, L., Ström, V., Berglund, L. A., et al. (2010). Making flexible magnetic aerogels and stiff magnetic nanopaper using cellulose nanofibrils as templates. *Nature Nanotechnology*, *5*, 584–588.

Pääkkö, M., Vapaavuori, J., Silvennoinen, R., Kosonen, H., Ankerdors, M., Lindström, T., et al. (2008). Long and entangled native cellulose I nanofibers allow flexible aerogels and hierarchically porous templates for functionalities. *Soft Matter*, *4*, 2492–2499.

Sehaqui, H., Salajková, M., Zhou, Q., & Berglund, L. A. (2010). Mechanical performance tailoring of tough ultra-high porosity foams prepared from cellulose I nanofiber suspensions. *Soft Matter*, *6*, 1824–1832.

Sescousse, R., Gavillon, R., & Budtova, T. (2011). Aerocellulose from cellulose-ionic liquid solutions: Preparation properties and comparison with cellulose-NMMO routes. *Carbohydrate Polymers*, *83*, 1766–1774.

Sescousse, R., Smacchia, A., & Budtova, T. (2010). Influence of lignin on cellulose–NaOH–water mixtures properties and on aerocellulose morphology. *Cellulose*, *17*, 1137–1146.

Sohn, B. H., & Cohen, R. E. (1997). Processible optically transparent block copolymer films containing superparamagnetic iron oxide naonclusters. *Chemistry of Materials*, *9*, 264–269.

Svagan, A. J., Berglund, L. A., & Jensen, P. (2011). Cellulose nanocomposite biopolymer foam-hierarchical structure effects on energy absorption. *ACS Applied Material and Interfaces*, *3*, 1411–1417.

Tang, B. Z., Geng, Y., Lam, J. W. Y., Li, B., Jing, X., Wang, X., et al. (1999). Processible nanostructured materials with electrical conductivity and magnetic susceptibility: Preparation and properties of maghemite/polyaniline nanocomposite films. *Chemistry of Materials*, *11*, 1581–1589.

Wei, T.-Y., Lu, S.-Y., & Chang, Y.-C. (2009). Transparent hydrophobic composite aerogels with high mechanical strength and low high-temperature thermal conductivies. *Journal of Physical Chemistry C*, *113*, 7424–7428.

Whang, K., Thomas, C. H., Healy, K. E., & Nuber, G. (1995). A novel method to fabricate bioabsorbable scaffolds. *Polymer*, *36*, 837–842.